JACS
JOURNAL OF THE AMERICAN CHEMICAL SOCIETY
Article
pubs.acs.org/JACS

Designed Synthesis, Structure, and Properties of a Family of Ferecrystalline Compounds $[(PbSe)_{1.00}]_m(MoSe_2)_n$

Colby L. Heideman,[†] Sara Tepfer,[‡] Qiyin Lin,[§] Raimar Rostek,[‡] Paul Zschack,[∥] Michael D. Anderson,[‡,⊥] Ian M. Anderson,[⊥] and David C. Johnson*[,‡]

[†]Department of Chemistry, Eastern Oregon University, La Grande, Oregon 97850, United States

[‡]Department of Chemistry, University of Oregon, Eugene, Oregon 97403, United States

[§]California Institute for Telecommunications and Information Technology, University of California, Irvine, California 92697, United States

[∥]Advanced Photon Source, Argonne National Laboratory, Argonne, Illinois 60439, United States

[⊥]Surface and Microanalysis Science Division, National Institute of Standards and Technology, Gaithersburg, Maryland 20899, United States

ABSTRACT: The targeted synthesis of multiple compounds with specific controlled nanostructures and identical composition is a grand challenge in materials chemistry. We report the synthesis of the new metastable compounds $[(PbSe)_{1.00}]_m(MoSe_2)_n$ using precursors each designed to self-assemble into a specific compound. To form a compound with specific values for m and n, the number of atoms within each deposited elemental layer was carefully controlled to provide the correct absolute number of atoms to form complete layers of each component structural unit. On low-temperature annealing, these structures self-assemble with a specific crystallographic orientation between the component structural units with atomically abrupt interfaces. There is rotational disorder between the component structural units and between $MoSe_2$ basal plane units within the $MoSe_2$ layers themselves. The lead selenide constituent has a distorted rock salt structure exactly m bilayers thick leading to peaks in the off-axis diffraction pattern as a result of the finite size of and rotational disorder between the crystallites. The in-plane lattice parameters of the PbSe and $MoSe_2$ components are independent of the value of m and n, suggesting little or no strain caused by the interface between them. These compounds are small band gap semiconductors with carrier properties dominated by defects and exhibit extremely low thermal conductivity as a result of the rotational disorder. The thermal conductivity can be tuned by varying the ratio of the number of ordered PbSe rock salt layers relative to the number of rotationally disordered $MoSe_2$ layers. This approach, based on controlling the local composition of the precursor and low temperature to limit diffusion rates, provides a general route to the synthesis of new compounds containing alternating layers of constituents with designed nanoarchitecture.

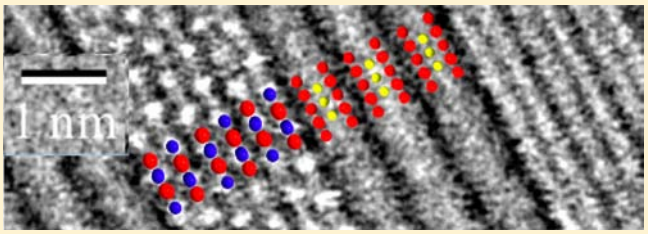

1. INTRODUCTION

The ability to design and implement the synthesis of new compounds has been fundamental to the advancement of chemistry and fields dependent on chemistry to make new compounds. Local coordination is used to predict potentially kinetic stable molecules, and strategies have been developed using designed precursor compounds with specific functionalities that are combined at relatively low temperatures to synthesize targeted molecules. Mild reaction conditions preserve key structural relationships present in the precursors as they react to form the final product, allowing complexity to rationally develop through the course of a many step synthesis. The addition of catalysts decreases activation energies for desired mechanistic pathways, and the use of protecting groups allows control of relative reaction rates between sites in a precursor. These techniques provide broad access to complex molecules, permitting, for example, many derivatives to be accessed around a single core parent structure. Systematic structural changes, for example varying the strength of an electron withdrawing group, provide both insight into what gives the core structure it is functionality and enables properties to be tuned to a desired application.

In contrast, synthesis in solid-state inorganic chemistry is much less developed, which has prevented the preparation of crystalline materials by design.[1] Working across the breadth of the periodic table, there are a wide variety of coordination numbers and bonding motifs for each element that make it difficult to predict the most stable of all possible extended structures.[2] Extended structures also involve the arrangement of large numbers of atoms ($\sim 10^{20}$ or more), and controlling their synthesis is more related to control of molecular packing in crystal structures than the synthesis of a particular molecule.[3] Because of slow diffusion rates in solids and the traditional large

Received: March 20, 2013
Published: July 2, 2013

dx.doi.org/10.1021/ja402819q | J. Am. Chem. Soc. 2013, 135, 11055−11062

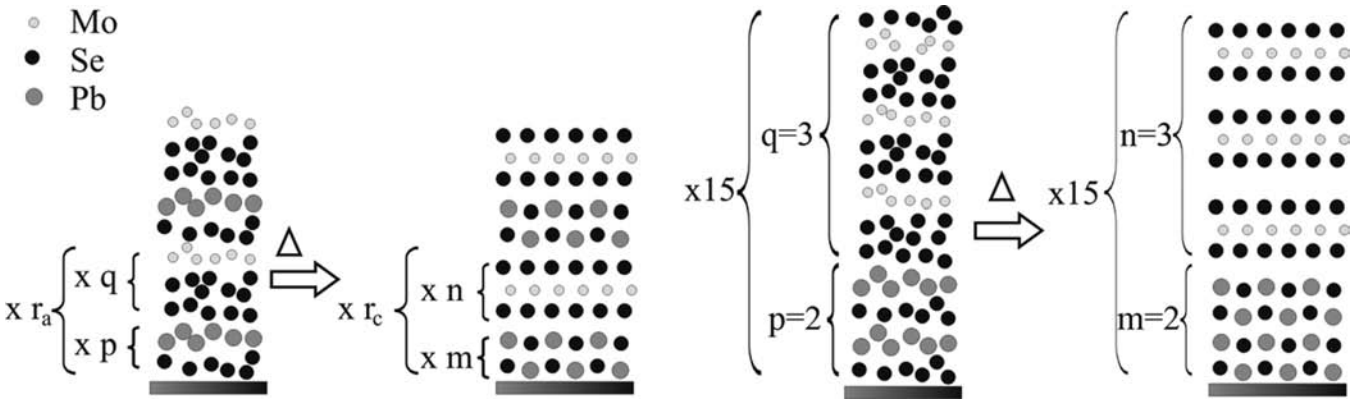

Figure 1. The schematic image on the left is a generic modulated precursor, which on annealing evolves into a targeted product. When the precursor is properly calibrated, the number of deposited layers (p and q) in the precursor will be equal to the number of structural units (m and n) of each constituent formed in the product, i.e., $p = m$ and $q = n$ and $r_a = r_c$, where r_a is the number of repeating units in the as deposited film and r_c is the number of repeating units in the crystalline film. A specific example is shown on the right for the precursor $p = 2$, $q = 3$ crystallizing into $m = 2$, $n = 3$.

size of solid reactants, high temperatures and long reaction times are typically required and usually result in thermodynamic products and little control of the reaction pathway.[4] These constraints have limited the number of compounds synthesized utilizing solid-state reactions, for the most part, to those that appear in equilibrium phase diagrams. Take, for example, the case of misfit layer compounds ($[(MX)_{1+\delta}]_n(TX_2)_m$, where M is Pb, Sn, Bi or a rare earth metal, T is a group IV or V transition metal, X is either S or Se, and δ is the degree of structural mismatch. Typically only a single member, $[(MX)_{1+\delta}]_1(TX_2)_1$ can be synthesized using traditional high-temperature synthesis.[5] In the rare cases when more than one family member has been synthesized, typically $[(MX)_{1+\delta}]_1(TX_2)_2$, it was achieved by varying the composition of the mixture of reactants, which serves as the primary tunable parameter for accessing new compounds in solid-state chemistry.[5−7] Choosing different values of n and m (Figure 1), however, can conceptually create an infinite family of structurally related compounds for each M and T. These chemically reasonable structures might be expected to be kinetically stable once prepared considering the stability of the known $m = n = 1$ compounds.

Here we report the use of designed layered elemental precursors (Figure 1) to prepare 18 new metastable compounds, $[(PbSe)_{1.00}]_m(MoSe_2]_n$, with an unusual ferecrystalline polymorph. We use the prefix fere, from the Latin 'fere' meaning almost, to describe these compounds' layered structures, which have in-plane crystallinity of each constituent and abrupt interfaces between each component but layer-to-layer misregistration and turbostratic disorder. Misfit layer compounds containing $MoSe_2$ as the transition-metal dichalcogenide have not been prepared using traditional solid-state synthesis techniques or any other approach, to our knowledge. The layered elemental precursors used herein, however, contain sufficient structural similarity in the modulation of the chemical composition of the final products to allow kinetic trapping of specific desired products, even when the products have identical stoichiometry but different structures.[8] The self-assembly of the specifically targeted $[(PbSe)_{1.00}]_m(MoSe_2]_n$ compound is facilitated by the short diffusion lengths in these precursors, which enables the reactions to proceed at low temperatures where diffusion rates are very small. The low diffusion rates prevent the formation of more thermodynamically stable products that involve longer-range diffusion of atoms. The ability to prepare many members of a large structurally related family of compounds allows structure and properties to be systematically investigated as a function of the number of structural units of each component. The self-assembly of designed precursors, since it only relies on controlling local compositions and relative diffusion lengths, might be a rather general approach to synthesizing a large number of different families of structurally related kinetically stable compounds. The structural modulation present in these compounds provides opportunities to explore thermal, electronic, and/or magnetic properties in the regime where the thickness of the constituent compounds are both above and below the fundamental length scale associated with the physical phenomena. In the regime where the layer thicknesses are below the critical thicknesses associated with the phenomena, the compounds would be expected to have properties distinct from that expected for a physical mixture of the components. The modulated structure of the target compounds also provides an opportunity to systematically explore and exploit chemical phenomena such as charge transfer between constituents as a means to tailor physical properties.

2. EXPERIMENTAL SECTION

The precursors were synthesized in a custom-built ultrahigh-vacuum deposition system with a pressure below 1×10^{-6} Torr during deposition.[9] Molybdenum and lead were deposited from an electron beam gun at a rate of 0.2 and 0.4 units/s, respectively, and selenium was deposited from an effusion cell at a rate of 0.5 units/sec. This rate was measured on a computer-controlled quartz crystal monitoring system where the crystal is located ∼1 cm from the substrate. Because tooling factors were not determined, the rate does not directly represent the amount of material deposited onto the substrate nor is it equivalent between sources, and therefore rates are reported in terms of units. For clarity, one unit is on the order of 1 Å. A motorized carousel rotates the substrate to each source, and elemental layers were deposited individually. A shutter over each vapor source controls the amount of material deposited onto the substrate during each deposition step. Samples were deposited on 100 oriented silicon substrates at ambient temperature for diffraction and thermal conductivity work and on fused silica for electrical measurements. Unless otherwise specified, samples were annealed at 400 °C for times ranging from 30 min to 1 h under an inert nitrogen atmosphere.

The composition of the precursors and compounds was determined by chemical analysis of the film using electron probe microanalysis. Data were collected at accelerating voltages of 10, 15, and 20 keV and

dx.doi.org/10.1021/ja402819q | J. Am. Chem. Soc. 2013, 135, 11055−11062

were modeled based on the expected penetration depth of the electrons at each accelerating voltage.[10−13]

The crystalline quality, orientation, and thickness of the films were evaluated by a high-resolution X-ray diffraction and reflectivity using a Bruker D8 Discover diffractometer with Cu Kα_1 radiation. The in-plane diffraction experiments were conducted at the Advanced Photon Source at Argonne National Lab at beamlines 33-BM and 33-ID.

Resistivity measurement was made using the van der Pauw technique at ambient temperature.[14,15] A shadow mask was used to create films with a Greek cross pattern. All electrical measurements were conducted on films deposited onto fused silica substrates to eliminate concerns about substrate contributions to the electrical measurements. Seebeck coefficients were determined using the integral method, where one side of the sample was left at ambient temperature and the other side cooled with a Peltier cooler.[16]

3. RESULTS AND DISCUSSION

Our approach to preparing specific members of the $[(PbSe)_{1.00}]_m(MoSe_2)_n$ family of misfit compounds was to prepare an amorphous precursor with compositional modulation comparable to that in the targeted compound. The compositional modulation of the precursor templates the targeted compound under diffusion constrained reaction conditions. We designed and calibrated the repeating unit of the precursor such that the relative and absolute amounts of atoms of each element within each region of the precursor correspond to the number of atoms needed to form complete structural units of each component on annealing. If too much or too little material is present, we found that the resulting partial layers disrupt the desired ordered structure. Figure 1 contains a schematic illustrating how specific precursors evolve into specific products.

3.1. Calibration. In order to synthesize precursors, physical vapor deposition was used to create the desired sequence of very thin elemental layers.[9] A calibration of the deposition process was performed to determine the deposition parameters necessary to produce modulated precursors with the correct amounts and ratio of elements. First the binary components, Pb−Se and Mo−Se, were first calibrated individually by preparing a series of samples where the amount of one element deposited was systematically increased, while the other was held constant. The amount of material deposited was monitored in situ on a quartz crystal balance, which provides a signal proportional to the deposition rate at the sample. The compositions of the resulting samples were measured using electron probe microanalysis utilizing accelerating voltages of 10, 15, and 20 keV.[11−13] Composition is proportional to the ratio of the relative thickness of each material as measured on the quartz crystal monitors. The thickness ratio of elements required to achieve a given composition is interpolated. This procedure yielded the deposition conditions required to obtain a 1:2 atomic ratio of Mo:Se for precursor layers designed to form $MoSe_2$ structural units and a 1:1 atomic ratio Pb:Se to form PbSe structural units. Compositions were chosen for the next step with a slight excess of selenium to compensate for selenium losses during annealing.

Once the relation between the measured thickness ratio and composition is established for the individual components, the absolute amount of material to form a single crystallized bilayer of rock salt or trilayer of transition-metal dichalcogenide was determined. PbSe has been reported to have a c-lattice parameter between 0.6124 and 0.616 nm.[17,18] The 2-H polymorph of $MoSe_2$ has been reported to have a c-lattice parameter of 1.2927 nm, yielding a single $MoSe_2$ structural unit thickness of 0.6464 nm.[17,19] Based on these data, a target thickness between 0.67 and 0.70 nm was established for the two amorphous components, about 0.05 nm thicker than the binary components, to compensate for loss of selenium on annealing and the density difference between the amorphous phase and the desired crystalline components. A series of samples was prepared where the number of times a Pb/Se bilayer is deposited per repeating unit was varied from 1 to 3 while holding the number of Mo/Se bilayers constant at 1, followed by a second series increasing the number of Mo/Se bilayers deposited from 1 to 3 while holding the number of Pb/Se bilayers constant at 1, shown in the graphical inset in the top plot of Figure 2. The thickness of the repeating unit deposited per cycle is determined by X-ray reflectometry measurements.

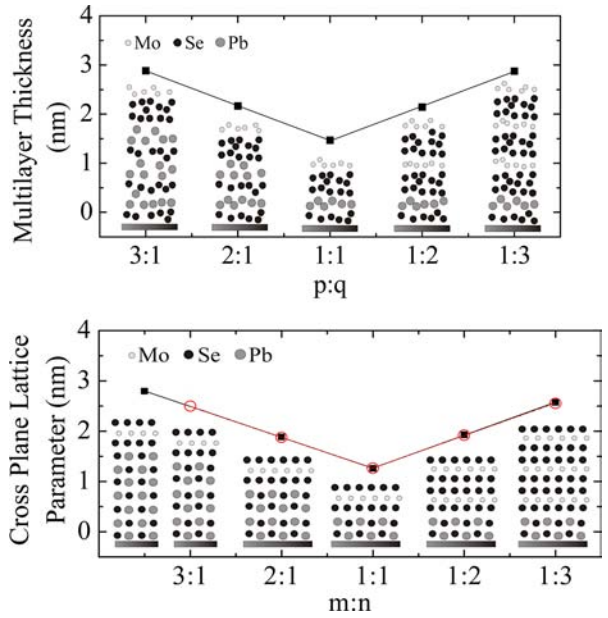

Figure 2. Plot of layer thickness versus number of deposition layers of Pb−Se and Mo−Se as initially deposited (top) and then after annealing at 400 °C for 30 min (bottom) using initial deposition parameters (solid squares) and adjusted deposition parameters (open circles). The first set of deposition parameters lead to 7 monolayers of PbSe forming when p = 3. For the second set, the values of p and q correspond to the values m and n after the samples are annealed to form the crystalline misfit compounds.

In Figure 2 we graph the measured layer thickness of different samples versus the number of Pb/Se layers (p) in the repeating unit and versus the number of Mo/Se layers (q) in the repeating unit. The squares represent multilayer thickness in samples made using the initial estimate of the appropriate deposition conditions. From the plot with increasing Pb−Se layers, a thickness of 0.71 nm was determined for the Pb−Se repeating unit and 0.76 nm for the Mo−Se repeating unit. From the plot with increasing Mo−Se layers, a thickness of 0.75 nm was determined for the Pb−Se repeating unit and 0.71 nm for the Mo−Se repeating unit. As expected, the slope of the line with increasing p is in agreement with the intercept of the line with increasing q, and the intercept of the line with increasing p is in agreement with the slope of the line with increasing q within experimental error.

After annealing at 400 °C for 30 min, the thickness of the repeating unit was again measured. In the series with increasing Mo−Se layers, a uniform increase in the c-lattice parameter of

dx.doi.org/10.1021/ja402819q | J. Am. Chem. Soc. 2013, 135, 11055−11062

the misfit compound is now observed at about 0.656 nm, which corresponds well with the expected thickness of a crystallized $MoSe_2$ basal plane unit. The intercept indicates thickness of 0.607 nm for the Pb/Se unit, in good agreement with thickness expected for two 100 planes of PbSe in a rock salt structure. After annealing the samples where the number of Pb−Se units was increased, however, the lattice parameter of the misfit compound formed from the p:q = 3:1 sample corresponded to that expected for $[(PbSe)_{1.00}]_{3.5}[MoSe_2]_1$, indicating that 7 (100) planes of PbSe formed when p = 3. This is only the second example of half integer values of m for ternary misfit layered compounds, and the first example with $m > 1.5$.[20] Decreasing the amount of Se and Pb per bilayer deposited in a second thickness calibration resulted in slopes and intercepts (Figure 2) that are in much better agreement with one another and closer to the expected values based on the lattice parameters of the binary compounds.

Once the deposition calibration is completed, any family member can be synthesized by varying the number of times each component layer is deposited between the other. Figure 3

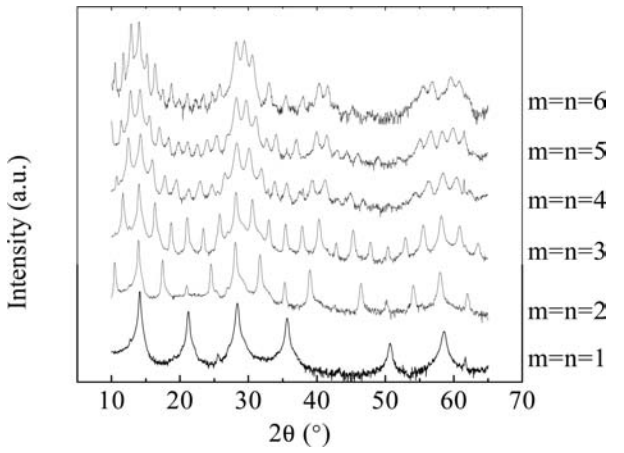

Figure 3. Diffraction data for six $[(PbSe)_{1.00}]_m[MoSe_2]_n$ compounds with identical stoichiometry. The vertical axis is log intensity, and the patterns are offset with arbitrary vertical displacements to separate them.

contains the diffraction scans of a series of isomers, $[(PbSe)_{1.00}]_m[MoSe_2]_n$, demonstrating the ability to control nanostructure while maintaining the same overall composition. Only 00l reflections are observed due to the strong preferred orientation that reflects the layered nature of the precursors. Table 1 contains the c-lattice parameters of 18 new misfit compounds, $[(PbSe)_{1.00}]_m[MoSe_2]_n$, including multiple preparations of the same compound. The c-lattice parameters vary slightly for different preparations of the same nominal composition, reflecting composition variations inherent to the deposition process used in this synthesis approach. For $[(PbSe)_{1.00}]_1[MoSe_2]_5$, a range of 0.06 nm was observed or 1.5% of the c-lattice parameter. This suggests that a range of stable compositions and modulation thicknesses exist for this compound. This synthesis approach allows for the rational synthesis of films with controlled composition and structure and may also allow more complicated stacking sequences to be made including graded and other nonrepeating layer sequences.

3.2. Reaction Mechanism. In order to explore the mechanism of the precursor self-assembling into product, an annealing study was conducted on samples that formed

Table 1. Lattice Parameters for 18 $[(PbSe)_{1.00}]_m[MoSe_2]_n$ Compounds[a]

m	n	c-lattice parameter (nm)	m	n	c-lattice parameter (nm)
1	1	1.273(4)	2	1	1.87 (3)
1	1	1.27(2)	2	1	1.857(2)
1	2	1.920(3)	2	2	2.531(3)
1	2	1.908(4)	2	3	3.182(5)
1	2	1.921(2)	2	4	3.834(4)
1	2	1.916(3)	2	5	4.496(7)
1	3	2.597(5)	3	1	2.490(3)
1	3	2.549(8)	3	1	2.481(9)
1	3	2.588(9)	3	1	2.49(2)
1	3	2.58(6)	3	1	2.47(2)
1	4	3.26(3)	3	1	2.465(5)
1	4	3.202(1)	3	1	2.479(5)
1	5	3.92(2)	3	1	2.47(1)
1	5	3.873(7)	3	1	2.48(1)
1	5	3.92(2)	3	3	3.820(3)
1	5	3.90(1)	3	3	3.798(5)
1	5	3.873(7)	4	1	3.05(9)
1	5	3.86(2)	4	1	3.09(3)
1	5	3.88(1)	4	4	5.04(1)
1	5	3.865(8)	4.5	1	3.417(7)
2	1	1.877(1)	5	1	3.72(3)
2	1	1.878(8)	5	1	3.64(9)
2	1	1.861(1)	5	5	6.32(1)
2	1	1.86(2)	6	6	7.65(4)

[a]The error for each lattice parameter is given in parentheses.

$[(PbSe)_{1.00}]_1[MoSe_2]_1$ and $[(PbSe)_{1.00}]_3[MoSe_2]_3$. They were annealed in a nitrogen drybox in 50 °C increments up to 650 °C for 30 min at each temperature. Diffraction data were collected following each annealing step. Figure 4 shows the diffraction scans obtained on the $[(PbSe)_{1.00}]_3[MoSe_2]_3$ sample. For both samples, significant long-range order is evident in the unannealed precursor reflecting the designed

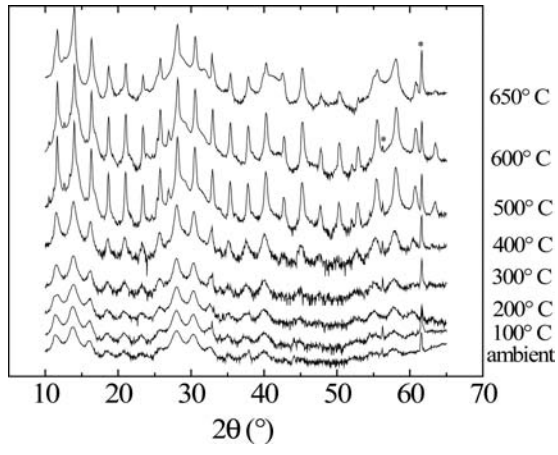

Figure 4. Diffraction patterns of a p = q = 3 sample as a function of annealing temperature as it evolves into the misfit compound $[(PbSe)_{1.00}]_3[MoSe_2]_3$. This sample is from a different deposition than the $[(PbSe)_{1.00}]_3[MoSe_2]_3$ sample used in Figure 3 and has a slightly different c-axis lattice parameter (see table 1) and peak intensities, probably reflecting a different concentration or distribution of defects. The vertical axis is the log of intensity to enhance the ability to see weak diffraction peaks. Patterns have been arbitrarily offset for visual clarity. * indicate peaks resulting from Si substrate.

dx.doi.org/10.1021/ja402819q | J. Am. Chem. Soc. 2013, 135, 11055−11062

nanoarchitecture. As the temperature is increased, there is little change in the c-lattice parameter, although the intensity of the reflections increases significantly with increased annealing temperature, indicating increasing order within the film. There is a sharp increase in peak intensity observed when the annealing temperature is increased from 400 to 500 °C for both samples, suggesting that there is more rapid growth of ordered crystalline domains within each component layer at these temperatures. Above this temperature for the $m = n = 1$ sample, the diffraction signal decreases from the superlattice peaks as the superstructure is destroyed and the components phase separate. For the $m = n = 3$ sample, the intensity continues to increase though 600 °C, indicating a more kinetically stable structure than the $m = n = 1$. This is somewhat surprising, as misfit compounds prepared from high-temperature annealing of the elements at the composition requisite for $m = n$, and hence expected to be the most thermodynamically stable compound, always form $m = n = 1$.

During the annealing process, the peak widths of rocking scans remain relatively constant up to 450 °C. Above this temperature, the preferred alignment within the film begins to increase dramatically, and the full width at half the maximum intensity decreases from 3.8° down to a minimum of 0.13° for the 006 reflection in $[(PbSe)_{1.00}]_3[MoSe_2]_3$ and from 4.6° to 1.5° for the 003 reflection in $[(PbSe)_{1.00}]_1[MoSe_2]_1$. This indicates an initial growth of the crystallites where degree of preferred orientation remains unchanged, followed by continued growth primarily parallel to the substrate. Such behavior is commonly observed in layered materials because of their preferred growth direction and the geometry of the layered precursor. Crystallites that are growing in directions other than parallel to the layering intersect with other grains sooner than those growing parallel, limiting the extent of their growth.[21]

3.3. Structure. *3.3.1. Cross-Plane Structure.* The compounds included in this report have different unit cell sizes and structures compared with related misfit layered compounds made using traditional methods. Along the *c*-axis, the structure consists of regularly repeating planes of atoms from the two interleaved constituents because of the near perfect preferred crystallographic orientation.[7,22,23] A linear increase in the c-lattice parameter is observed as m and n are increased. The change per additional Se−Mo−Se structural unit is 0.660(4) and 0.654(1) for $m = 1$ and 2, respectively, slightly larger than the thickness of a $MoSe_2$ layer found in bulk $MoSe_2$ (0.646 nm).[24] The change in lattice parameter as m is incremented is 0.605(3), which is consistent with adding a bilayer of (001) planes of PbSe as m is incremented by 1. The 0.605 per bilayer of PbSe is slightly smaller than the unit cell size of bulk PbSe (0.6124−0.616 nm).[17,18]

3.3.2. In-Plane Structure. The in-plane structure was analyzed using grazing incidence in-plane diffraction. A representative pattern is shown in Figure 5 for $[(PbSe)_{1.00}]_3[MoSe_2]_3$. Because the structures are incommensurate along the *a* and *b* axes, completely independent families of diffraction maxima are evident in the in-plane pattern. On average among all of the compounds that were prepared, the a-lattice parameter for PbSe was determined to be 0.617(5) nm, slightly larger than the 0.6124−0.616 nm unit cell reported for bulk PbSe, and for $MoSe_2$ it was determined to be 0.332(2) nm, also slightly larger than the 0.3289 lattice parameter reported for bulk $MoSe_2$.[24] Within the accuracy of the measurement, a square in-plane structure was found for PbSe instead of a distortion to rectangular symmetry observed for traditional misfit compounds.[7,25,26] While there is some variation in the lattice parameter from one compound to another, no trend is evident as the thickness of each block is increased. This suggests that, despite the lattice mismatch, there is little or no strain present at the interface.[27] The degree δ of structural misfit was calculated from the in-plane lattice parameter of both components, and δ was found to be 1.00(1). This value is significantly smaller than previously reported values (1.07−1.28).[7,28,29] The components also have different domain sizes in the *a*−*b* plane, as determined from Scherrer analysis of the peak broadening and summarized in Table 2. Grain sizes were calculated using the (202) reflections in PbSe and the (103) reflections in $MoSe_2$. The domains for both components are small, on the order of about 10 nm for PbSe and 5 nm for $MoSe_2$, and independent of the values of m and n.

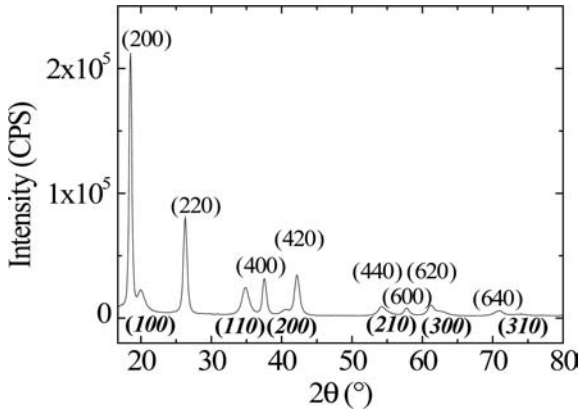

Figure 5. In-plane diffraction from $[(PbSe)_{1.00}]_3(MoSe_2)_3$. Miller indices above the pattern are centered above reflections from PbSe, those below the pattern are indices of the $MoSe_2$ reflections.

Table 2. In-Plane Structure of Seven $[(PbSe)_{1.00}]_m[MoSe_2]_n$ Compounds

	a-lattice parameter (nm)		grain size (nm)	
structure	PbSe	$MoSe_2$	PbSe	$MoSe_2$
$m = 1, n = 1$	0.616 ± 0.001	0.332 ± 0.002	9 ± 3	4 ± 1
$m = 1, n = 1$	0.618 ± 0.001	0.332 ± 0.001	9 ± 3	5 ± 1
$m = 3, n = 1$	0.614 ± 0.001	0.331 ± 0.007	7 ± 2	5 ± 1
$m = 3, n = 3$	0.616 ± 0.001	0.331 ± 0.001	8 ± 2	4 ± 1
$m = 4, n = 4$	0.616 ± 0.001	0.332 ± 0.001	10 ± 2	4 ± 1
$m = 5, n = 5$	0.615 ± 0.001	0.333 ± 0.002	9 ± 2	4 ± 1
$m = 5, n = 5$	0.618 ± 0.001	0.335 ± 0.001	12 ± 3	4 ± 1
$m = 6, n = 6$	0.617 ± 0.001	0.333 ± 0.001	10 ± 3	4 ± 1

3.3.3. Off-Axis Structure. Off-axis diffraction scans (Figure 6) contain two independent families of broad diffraction maxima near positions expected for PbSe and $MoSe_2$. The $MoSe_2$ reflections remain essentially constant for all samples regardless of the values of m and n. This reflects the lack of coherence between the layers, with coherence lengths calculated to be less than twice the thickness of a single structural unit of $MoSe_2$.

For PbSe, unexpected reflections appear when $m > 1$ that are a consequence of the finite crystal size present in the PbSe layers and the rotational disorder between these layers. The position of these unexpected reflections is independent of n and hence the c-lattice parameter. These finite size reflections in the

dx.doi.org/10.1021/ja402819q | J. Am. Chem. Soc. 2013, 135, 11055−11062

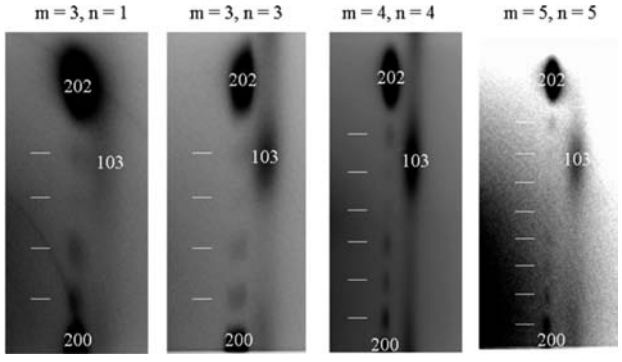

Figure 6. Off-axis diffraction data for four $[(PbSe)_{1.00}]_m[MoSe_2]_n$ samples. Because of the lack of coherence between layers, superstructure along (00l) is not observed. The intense reflections correspond to the individual components and are near reflections expected for PbSe ((200) and (202)) and $MoSe_2$ (103). The weak satellite reflections (indicated by white dashes) between the PbSe (200) and (202) reflections result from the finite size of the PbSe crystallites. The number of reflections corresponds to $2m - 2$ (where m is the number of rock salt bilayers) and is independent of the thickness of the $MoSe_2$ component.

c direction of the PbSe crystalline domains are a consequence of the domains terminating with atomic abruptness, containing a fixed number of atomic planes determined only by the value of m and having the same crystallographic orientation along the c-axis. The number of minima between Bragg reflections resulting from the discrete number of planes can be readily shown to equal $n - 1$ by considering the interference of waves scattering from each plane. In each case shown in Figure 6, an even number of atomic planes are present in the rock salt layer, leading to an odd number of minima. These minima are equally separated in reciprocal space, such that they correspond to integer value indexing when the finite crystal size is determined using Bragg's law, and the positions of the maxima are hence predicted at half integer values. Table 3 shows the size calculated for each finite PbSe block compared to the size predicted from the regular increase in the unit cell shown in Figure 6.

Table 3. Comparison of the Size the PbSe Rock Salt Crystallites Along the c-Axis[a]

m	column A (nm)	column B (nm)
2	1.26(5)	1.23(3)
3	1.81(4)	1.84(5)
4	2.42(6)	2.45(5)
5	2.96(7)	3.07(5)

[a]Calculated from the position of reflection peaks in the off-axis diffraction data (Figure 6) caused by the finite size of the crystallites (column A) and from the thickness of the rock salt layers calculated from the c-lattice parameters contained in Table 1 as m is varied (column B).

High-resolution STEM-HAADF images (Figure 7) confirm the lack of long-range crystallographic order between $MoSe_2$ structural units, between $MoSe_2$ and PbSe structural units, and between PbSe structural units in different repeating units along the c axis. The lack of long-range periodicity within the $MoSe_2$ layers reflects the relatively weak van der Waals interactions between $MoSe_2$ trilayers. The decrease in free energy resulting from forming ordered crystals is not sufficient to induce

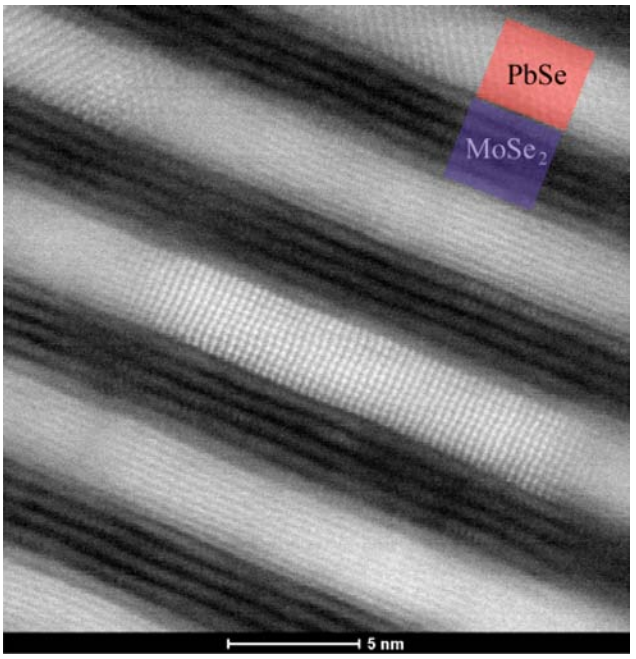

Figure 7. High-resolution STEM-HAADF image of $[(PbSe)_{1.00}]_5(MoSe_2)_5$.

ordering of the trilayers at the annealing temperatures investigated, probably due to the low solid-state diffusion rates. The rock salt layers are single crystals for their full thickness, with the (00l) planes of the rock salt aligned parallel with the (00l) planes of the dichalcogenide. There appears to be a random alignment between the a–b planes of the dichalcogenide and the rock salt. The grain boundaries of an individual rock salt layer do not align with grain boundaries in the dichalcogenide.

The analysis of the STEM and diffraction data suggests an unusual interplay between crystallographic order and disorder in this family of $[(PbSe)_{1.00}]_m[MoSe_2]_n$ compounds. These compounds have in-plane crystallinity resulting in $hk0$ diffraction peaks and abrupt interfaces between the constituents and periodic atomic planes of atoms along the c-axis resulting in (00l) diffraction patterns. The lack of (hkl) (h, $k \neq 0$; $l \neq 0$) diffraction implies the lack of long-range order in these directions, which results from layer-to-layer misregistration or turbostratic disorder between the structural units of the components and between the structural units of $MoSe_2$. This combination leads us to suggest the term ferecrystals (from Latin fere, meaning almost), to describe the unusual structure of these new compounds, poised between the crystalline and amorphous states.

3.4. Properties. Resistivity measurements show that these compounds are semiconductors that exhibit a range of conductivities that depend on the defect levels in the films with activation energies between 0.15 and 0.20 eV extracted from the variable-temperature conductivity for $[(PbSe)_{1.00}]_1(MoSe_2)_1$. The carrier concentration was found to strongly depend on annealing conditions as well as the initial deposition conditions. Carrier concentrations in general decreased, and carrier mobility increased with annealing in controlled selenium partial pressures. As mentioned earlier, there is a significant phase width for each stable compound leading to variation in the composition and structure for each stable compound in the $[(PbSe)_{1.00}]_m[MoSe_2]_n$ family. This

dx.doi.org/10.1021/ja402819q | J. Am. Chem. Soc. 2013, 135, 11055–11062

makes characterization and interpretation of the electrical properties of these materials nontrivial, and the details will be discussed in a future paper.

We have previously reported exceptionally low thermal conductivity resulting from the turbostratic disorder present between layers in transition-metal dichalcogenides.[30−32] It was therefore expected that these ferecrystals would exhibit similarly low thermal conductivity due to the rotational disorder present between layers. Traditionally, low thermal conductivity in layered materials was believed to arise from scattering at the interfaces, leading to decreasing thermal conductivity with increasing interface density. For the ferecrystals reported here, the interface density is not nearly as important as the ratio of the two components. For example, the thermal conductivity is essentially identical for compounds $m = n = 1, 2, 3$. This suggests the film can be treated as a composite of the two materials leading to a total thermal conductivity being the sum of the series thermal conductivity of the individual components. This leads to a total thermal conductivity of $(m + n)/\Lambda_{multilayer} = m/\Lambda_{PbSe} + n/\Lambda_{MoSe_2}$, where m and n are the number of PbSe and $MoSe_2$ layers, respectively, and Λ is the thermal conductivity. Figure 8 shows a plot of the measured thermal conductivity

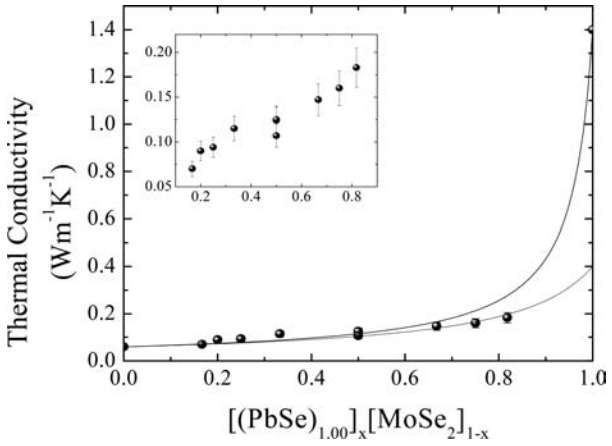

Figure 8. Plot of thermal conductivity versus PbSe percent. The solid line is the prediction from the measured values of the binary compounds. The lighter curve is a best fit to the composite model described in the manuscript, which predicts the thermal conductivity of the PbSe layer in the ferecrystals to be 0.4 Wm^{-1} K^{-1}. Inset zooms in leaving off the pure binary components and has the same units as the primary figure.

versus composition and several different approaches to fit the data to the above equation. The solid line uses experimental values for the thermal conductivity of films of PbSe and $MoSe_2$ to calculate the thermal conductivity of the new ferecrystalline compounds. While the curve approximates the thermal conductivity of $MoSe_2$-rich ferecrystals, it overestimates the thermal conductivity of PbSe-rich ferecrystals. This is not surprising, because the grain size of the PbSe film used in the thermal conductivity measurement was calculated to be 30(4) nm using the Scherrer equation, much larger than the thickness of the PbSe layers within the ferecrystal. The dotted line in Figure 8 is a fit, where the thermal conductivity of PbSe was treated as a variable. The thermal conductivity calculated for PbSe is 0.4 Wm^{-1} K^{-1}, significantly lower than the 1.4 Wm^{-1} K^{-1} measured for the film of pure PbSe prepared as part of this study and significantly lower than previous measurements of PbSe, which range from 1.6 Wm^{-1} K^{-1} for nanostructured PbSe/PbTe to 9 Wm^{-1} K^{-1} for bulk PbSe.[33] Given the decrease in grain size, which would be expected to decrease the mean free path for phonons significantly, this thermal conductivity value seems reasonable. The low thermal conductivities found in ferecrystalline compounds make them attractive as potential thermoelectric materials. This will require the ability to rationally control carrier concentrations via either by controlled introduction of dopants or by taking advantage of charge transfer from one constituent to the other, referred to as modulation doping in the 3−5 semiconductor literature. The ability to prepare many members in a family of compounds, as illustrated herein, provides the possibility to also tune properties using defined nanostructure.

4. CONCLUSION

We have successfully prepared precursors, which self-assembled at low temperatures to the targeted kinetically stable $[(PbSe)_{1.00}]_m[MoSe_2]_n$ compounds. A systematic calibration procedure allows the preparation of layered precursors that form specific members in this family of compounds on annealing. These compounds have in-plane crystallinity with abrupt interfaces between the constituents and the periodic atomic planes of atoms along the c-axis. There is no long-range order in (hkl) $(h, k \neq 0; l \neq 0)$ directions, which results from layer-to-layer misregistration or turbostratic disorder between the structural units of the components and between the structural units of $MoSe_2$. These compounds were found to be semiconductors with very low thermal conductivities that could be rationalized using a simple composite model of the constituents. The synthesis approached used herein relies on controlling local compositions and diffusion distances with the precursors and hence should generally applicable to many other systems. The ability to prepare many compounds within a family of structurally related materials should allow thermal, electronic, and magnetic properties to be manipulated using the thickness, the ratio of the constituent compounds, or charge transfer between the constituents. It also provides an opportunity for theory to both explain the trends in properties observed and predict the properties of compounds within the family yet to be prepared.

■ AUTHOR INFORMATION

Corresponding Author

davej@uoregon.edu

Notes

The authors declare no competing financial interest.

■ ACKNOWLEDGMENTS

The authors thank C. Chiritescu and D. G. Cahill for thermal conductivity measurements and Jenia Karapetrova for assistance in synchrotron XRD data collection. The authors acknowledge support from the National Science Foundation under grant DMR 0907049 and MRI 0923577. D.C.J. acknowledges support from the National Science Foundation through CCI grant no. CHE-1102637 and C.L.H. and M.D.A. acknowledge support from the University of Oregon's National Science Foundation IGERT Fellowship Program under grant no. DGE-0549503. Use of the Advanced Photon Source was supported by the U.S. Department of Energy, Office of Science, Office of Basic Energy Sciences, under contract no. DE-AC02-06CH11357.

REFERENCES

(1) Stein, A.; Keller, S. W.; Mallouk, T. E. *Science* **1993**, *259*, 1558.
(2) DiSalvo, F. J. *Science* **1990**, *247*, 649.
(3) Russell, V. A.; Ward, M. D. *Chem. Mater.* **1996**, *8*, 1654.
(4) West, A. R. *Basic Solid State Chemistry*; 2nd ed.; John Wiley & Sons: Hoboken, NJ, 1999.
(5) Wiegers, G. A.; Meerschaut, A. *Mater. Sci. Forum* **1992**, *100−101*, 101.
(6) Wiegers, G. A. *Prog. Solid State Chem.* **1996**, *24*, 1.
(7) Oosawa, Y.; Gotoh, Y.; Akimoto, J.; Tsunoda, T.; Sohma, M.; Onoda, M. *Jpn. J. Appl. Phys., Part 2* **1992**, *31*, L1096.
(8) Noh, M.; Johnson, C. D.; Hornbostel, M. D.; Thiel, J.; Johnson, D. C. *Chem. Mater.* **1996**, *8*, 1853.
(9) Fister, L.; Li, X.-M.; McConnell, J.; Novet, T.; Johnson, D. C. *J. Vac. Sci. Technol., A* **1993**, *11*, 3014.
(10) Phung, T. M.; Jensen, J. M.; Johnson, D. C.; Donovan, J. J.; McBurnett, B. G. *X-Ray Spectrom.* **2008**, *37*, 608.
(11) Pouchou, J. L.; Pichoir, F. *Electron Probe Quant.* **1991**, 31.
(12) Donovan, J. J.; Tingle, T. N. *J. Microsc. Soc. Am.* **1996**, *2*, 1.
(13) Pouchou, J.-L. *Microchim. Acta* **2002**, *138*, 133.
(14) van der Pauw, L. J. *Philips Res. Rep.* **1958**, *13*, 1.
(15) van der Pauw, L. J. *Philips Tech. Rev.* **1958**, *20*, 220.
(16) Kumar, S. R. S.; Kasiviswanathan, S. *Rev. Sci. Instrum.* **2008**, *79*, 024302/1.
(17) Swanson, H. E.; Gilfrich, N. T.; Ugrinic, G. M. *Natl. Bur. Stand. Circ. (U. S.)* **1955**, *5*, 75.
(18) Hummer, K.; Gruneis, A.; Kresse, G. *Phys. Rev. B: Condens. Matter Mater. Phys.* **2007**, *75*, 195211/1.
(19) Cech, F.; Rieder, M.; Vrana, S. *Neues Jahrb. Mineral., Monatsh.* **1973**, 433.
(20) Cario, L.; Lafond, A.; Palvadeau, P.; Deudon, C.; Meerschaut, A. *J. Solid State Chem.* **1999**, *147*, 58.
(21) Van der Drift, A. *Philips Res. Rep.* **1967**, *22*, 267.
(22) Roesky, R.; Meerschaut, A.; Rouxel, J.; Chen, J. *Z. Anorg. Allg. Chem.* **1993**, *619*, 117.
(23) Oosawa, Y.; Gotoh, Y.; Onoda, M. *Chem. Lett.* **1989**, 1563.
(24) Bronsema, K. D.; De Boer, J. L.; Jellinek, F. *Z. Anorg. Allg. Chem.* **1986**, 540.
(25) Auriel, C.; Roesky, R.; Meerschaut, A.; Rouxel, J. *Mater. Res. Bull.* **1993**, *28*, 247.
(26) Auriel, C.; Meerschaut, A.; Roesky, R.; Rouxel, J. *Eur. J. Solid State Inorg. Chem.* **1992**, *29*, 1079.
(27) Osbourn, G. C. *IEEE J. Quantum Electron.* **1986**, *QE-22*, 1677.
(28) Lafond, A.; Deudon, C.; Meerschaut, A.; Sulpice, A. *Eur. J. Solid State Inorg. Chem.* **1994**, *31*, 967.
(29) Gotoh, Y.; Akimoto, J.; Goto, M.; Oosawa, Y.; Onoda, M. *J. Solid State Chem.* **1995**, *116*, 61.
(30) Chiritescu, C.; Cahill, D. G.; Nguyen, N.; Johnson, D.; Bodapati, A.; Keblinski, P.; Zschack, P. *Science* **2007**, *315*, 351.
(31) Chiritescu, C.; Cahill, D. G.; Heideman, C.; Lin, Q.; Mortensen, C.; Nguyen, N. T.; Johnson, D.; Rostek, R.; Bottner, H. *J. Appl. Phys.* **2008**, *104*, 033533/1.
(32) Lin, Q.; Heideman, C. L.; Nguyen, N.; Zschack, P.; Chiritescu, C.; Cahill, D. G.; Johnson, D. C. *Eur. J. Inorg. Chem.* **2008**, 2382.
(33) Greig, D. *Phys. Rev.* **1960**, *120*, 358.